ACS APPLIED MATERIALS & INTERFACES

Research Article

www.acsami.org

Bifunctional Nanocatalyst Based on Three-Dimensional Carbon Nanotube–Graphene Hydrogel Supported Pd Nanoparticles: One-Pot Synthesis and Its Catalytic Properties

Zheye Zhang,[†,∥] Tai Sun,[†,§,∥] Chen Chen,[†] Fei Xiao,*[,†] Zheng Gong,*[,‡] and Shuai Wang*[,†]

[†]School of Chemistry & Chemical Engineering, Huazhong University of Science and Technology, Wuhan 430074, People's Republic of China

[‡]Western Digital Corporation, 5863 Rue Ferrari, San Jose, California 95138, United States

[§]Chongqing Institute of Green and Intelligent Technology, Chinese Academy of Sciences, Chongqing 400714, People's Republic of China

Supporting Information

ABSTRACT: We reported the development of a new type of bifunctional nanocatalyst based on three-dimensional (3D) macroscopic carbon nanotube (CNT)–graphene hydrogel (GH) supported Pd nanoparticles (i.e., Pd–CNT–GH) and explored its practical application in catalytic reduction of *p*-nitrophenol to *p*-aminophenol. The 3D Pd–CNT–GH was synthesized by a facile one-pot self-assembled approach through hydrothermal treatment of a mixed aqueous precursor solution of $PdCl_4^{2-}$, CNT, and graphene oxide (GO). Under the appropriate condition, the spontaneous redox reaction between precursor $PdCl_4^{2-}$ and CNT–GO as well as the self-assembly of macroscopic CNT–GH occurs simultaneously, leading to the formation of 3D Pd–CNT–GH. Because of the unique structural and functional properties of different components in the nanocatalyst and the synergistic effect between them, the as-prepared Pd–CNT–GH exhibits superior catalytic performance toward the reduction of *p*-nitrophenol to *p*-aminophenol, with 100% conversion within 30 s, even when the content of Pd in it is as low as 2.98 wt %. Moreover, after 20 successive cycles of reactions, the reaction time still keeps within 46 s. Therefore, the rational design of 3D macroscopic graphene-based nanohybrid material supported highly catalytically active nanoparticles, combined with the facile one-pot self-assembled strategy, provide a universal platform to fabricate desired 3D multifunctional nanomaterials that can be used in a broad range of catalysis, environmental protection, energy storage and conversation, drug delivery, chemical and biological sensing, and so forth.

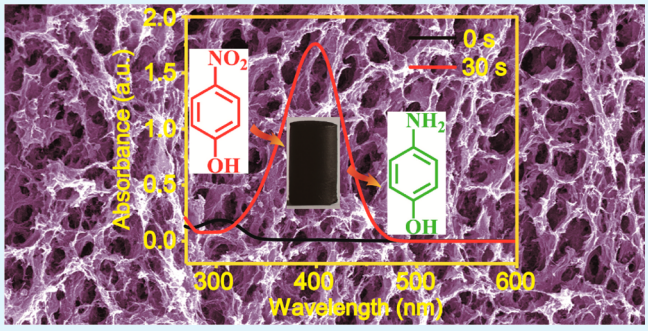

KEYWORDS: *palladium nanoparticles, carbon nanotube, graphene hydrogel, one-pot self-assembly, catalysis, p-nitrophenol*

1. INTRODUCTION

In the past two decades, functional nanomaterials with unique physical and chemical properties have attracted scientific interest for their potential applications in diverse areas such as gas sensor, biosensor, energy conversion, heterogeneous catalysis, and fuel cells.[1−3] Especially, bifunctional nanocatalysts that comprise both active metal nanoparticles (NPs) and high surface area support have been intensively investigated due to their tailorability and functionality in both the catalytic nanometal and the support material.[4] For catalytic application of bifunctional nanocatalysts, noble metal NPs with ultrafine sizes play an important role due to their large surface area and the number of edge and corner atoms, which greatly improve their catalytic properties. In parallel, tremendous effort has also been devoted into designing and fabricating catalyst support, which can restrict the aggregation of metal NPs on it,[5−8] and therefore increase the catalytic activity of metal NPs. Up to now, several works have been focused on decorating metal NPs on carbon-based nanomaterials such as carbon fiber, carbon microsphere, and carbon nanotube (CNT).[9,10] These carbon-based materials exhibit large surface area, excellent mechanical and electrical properties, which not only function as barriers to prevent encapsulated NPs from coalescence, but also improve the chemical and thermal stability, as well as enhance the electrical conductivity of functional materials.[11−14]

As an intriguing two-dimensional carbon nanomaterial, graphene has recently been the subject of intense research, due to its extraordinary chemical and mechanical properties that are comparable to or even better than CNT.[15] Graphene nanosheets also exhibit excellent conductivity for electron capture and transport, and unique interaction with catalyst particles, which make them quite promising for catalysis.[16−18]

Received: August 31, 2014
Accepted: November 6, 2014
Published: November 6, 2014

Nevertheless, for the practical application of graphene-supported metal nanocatalysts, the primary problem is the serious $\pi-\pi$ stacking interactions between graphene nanosheets, which lead to serious aggregation and restacking of graphene nanosheets, and consequently decrease their specific surface area and block active catalytic sites on graphene.[19] On the other hand, it is difficult to synthesize stable metal NPs that anchored on graphene supports because the metal NPs tend to aggregate into larger species, especially under the harsh reaction conditions such as high temperatures and subsequent detoxification processes, which significantly hamper their catalytic activity. Therefore, it still remains a challenge to develop facile and reliable synthetic routes to structure-controlled, highly efficient, and reusable catalysts.

In this Article, we report a facile one-pot self-assembled approach to fabricate highly active and durable bifunctional nanocatalyst based on three-dimensional (3D) CNT−reduced graphene oxide (rGO) hydrogel supported Pd NPs. Ultrafine Pd NPs were in situ grown on the surface of CNT−GO nanohybrid by the spontaneous redox reaction between $PdCl_4^{2-}$ and CNT−GO hybrid under mild condition. A desired three-dimensional (3D) hierarchically porous CNT−rGO hydrogel supported Pd NP (Pd−CNT−rGO hydrogel) then was obtained by hydrothermal treatment of Pd−CNT−GO aqueous dispersion. The synthesis does not necessitate any chemical reducing or capping agents. The 3D CNT−rGO hydrogel possesses large surface area and ample volume with hierarchically porous structure. Furthermore, the introduction of highly conductive CNT into rGO sheets not only prevents the $\pi-\pi$ stacking interactions between graphene nanosheets, but also greatly improves the electron-transfer rate and dramatically enhances the durability of the Pd catalyst. Because of the unique structural and functional properties of different components in the nanocatalyst and the synergistic effect between them, the as-prepared nanocatalyst exhibits remarkably high and stable catalytic activity in the reduction of *p*-nitrophenol. The reduction of *p*-nitrophenol by $NaBH_4$ to *p*-aminophenol could be finished in only 30 s at room temperature, even when the content of Pd in it is as low as 2.98 wt %, and the reaction time still keeps within 46 s after 20 successive cycles of reactions.

2. EXPERIMENTAL SECTION

2.1. Preparation of Pd−CNT−rGO Nanocomposite. Natural graphite and multiwall CNT (length 10−30 μm, outside diameter 10−20 nm) were obtained from XF NANO, Inc. (China). For the preparation of Pd−CNT−GO precursor, GO was synthesized from natural graphite by the modified Hummers method.[20,21] 30 mg of CNT was then added to 2 mg mL^{-1} homogeneous GO aqueous dispersion (30 mL). Subsequently, H_2PdCl_4 aqueous solution (4 mL, 10 mM) was added to the CNT−GO dispersion and maintained in an ice bath under sonication for approximately 30 min. In a typical synthesis of Pd−CNT−rGO hydrogel, the precursor solution was sealed in a 50 mL Teflon-lined autoclave and maintained at 180 °C for 12 h. After being cooled in room-temperature air with natural convection, a black gel-like 3D cylinder was obtained. The size of the hydrogel could be freely adjusted by changing the volume of the GO aqueous dispersion. The 3D Pd−rGO hydrogel was fabricated under a similar procedure.

2.2. Characterization. Scanning electron microscopy (SEM) images were obtained on a field-emission scanning electron microscope (GSM6510LV, JEOL, Japan). Transmission electron microscopy (TEM) and high-resolution transmission electron microscopy (HRTEM) images were obtained using a TECNAI G2 20 U-Twin instrument (Netherlands) operated at an acceleration voltage of 200 kV. The samples suspended in ethanol were drop-casted onto a carbon-coated 200-mesh copper grid and subsequently dried at room temperature. X-ray photoelectron spectroscopy (XPS) measurements were performed on a VG ESCALAB 250 spectrometer (UK) using an Al Kα X-ray source (1486 eV), X-ray radiation (15 kV and 10 mA), and hemispherical electron energy analyzer. All of the binding energies were calibrated according to the reference energy of C 1s (C 1s = 284.6 eV). X-ray powder diffraction (XRD) measurements were performed on a diffractometer (X' Pert PRO, Panalytical B.V., Netherlands) equipped with a Cu Kα radiation source. The Pd content was determined using a microwave plasma-atom emission spectrometer (MP-AES, Agilent 4100, U.S.). UV−vis measurements were conducted on a Specord 50 UV−vis spectrophotometer (Germany). Nitrogen adsorption/desorption isotherms were obtained at 77 K on an accelerated surface area and porosimetry system (ASAP 2020, U.S.) to measure the surface area of the films using the Brunauer−Emmett−Teller (BET) method.

2.3. Study of the Catalytic Properties. *p*-Nitrophenol (3 mL, 0.1 mM) was mixed with a freshly prepared aqueous solution of $NaBH_4$ (0.1 mL, 0.3 M). The as-prepared Pd−CNT−rGO nanocatalysts (5 mg) were added under constant magnetic stirring. UV−vis absorption spectra were recorded to monitor the change in the reaction mixture.

3. RESULTS AND DISCUSSION

Figure 1 illustrates the fabrication process of Pd−CNT−rGO hydrogel. First, the homogeneous CNT−GO dispersion has

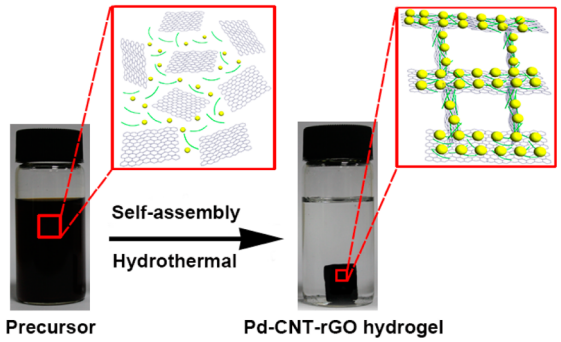

Figure 1. Fabrication process of the Pd−CNT−rGO hydrogel.

been obtained under the sonication treatment (Supporting Information Figure S1a), where the CNTs are well dispersed by amphiphilic GO solution and adsorbed onto the GO surface through $\pi-\pi$ attractions.[22] H_2PdCl_4 aqueous solution was subsequently added into CNT−GO dispersion by mixing together in an ice bath for approximately 30 min. According to previous studies, the reduction potential of $PdCl_4^{2-}$ is about +0.83 V vs SCE, which is much higher than the oxidation potential of GO (+0.48 V vs SCE)[23] and CNT (+0.5 V vs SHE).[24−27] Therefore, the spontaneous oxidation and reduction of GO/$PdCl_4^{2-}$ and CNT/$PdCl_4^{2-}$ will occur in their precursor solution, leading to the formation of desired Pd NPs decorated CNT−GO nanocomposite, where the ultrafine Pd NPs are well-dispersed on the surface of CNT−GO nanocomposite (Supporting Information Figure S1b). The size distribution histogram is based on more than 500 particles, and the average particle size of the Pd NPs is about 2−3 nm. The 3D Pd−CNT−rGO hydrogel was obtained by hydrothermal treatment of the Pd−CNT−GO aqueous dispersion. By the weak interactions, such as van der Waals forces, hydrogen bonding, $\pi-\pi$ stacking, and inclusion interactions, between different components, the macroscopic Pd−CNT−rGO nanohybrid cylinder was formed. The as-obtained Pd−CNT−rGO

nanocomposite material exhibits well-defined interconnected 3D porous network, and the pore walls consist of thin layers of stacked graphene nanosheets (Figure 2a). The partial

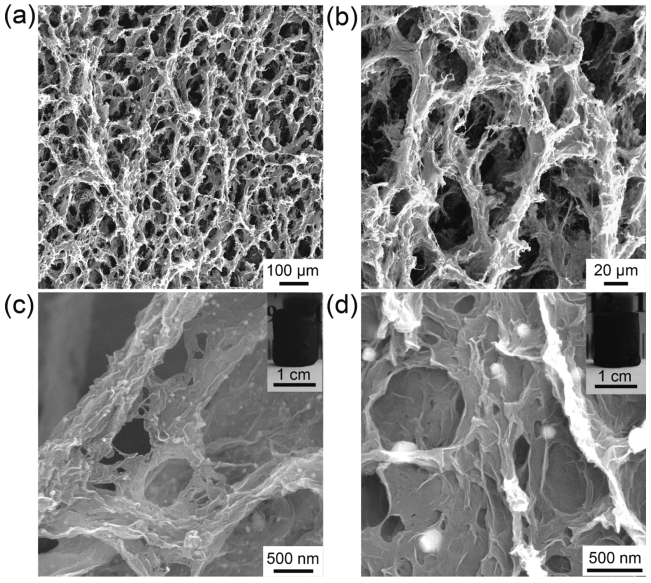

Figure 2. SEM images of (a–c) Pd–CNT–rGO nanocomposite, and (d) Pd–rGO nanocomposite.

coalescing or overlapping of graphene sheets results in the formation of cross-linking sites of the hybrid framework, and the pore sizes of the network are in the range from several micrometers to submicrometer (Figure 2b). From the high magnified SEM images of both Pd–CNT–rGO (Figure 2c) and Pd–rGO composites (Figure 2d), it is found that Pd NPs are uniformly anchored onto the graphene nanosheets, and no aggregated NPs can be observed from the supports. The BET specific surface area of Pd–CNT–rGO composite is up to 286.7 $m^2 g^{-1}$ (Supporting Information Figure S2a), which is much higher than that of Pd–rGO composite (173.4 $m^2 g^{-1}$, Supporting Information Figure S2b). Taking into account that the CNTs can interact with rGO sheets and distribute sparsely on the entire sheet surface, they will act as the spacer to partially prevent the aggregation of the graphene sheets, and to a great extent increase the specific surface area. TEM has further been employed to characterize the nanostructure of Pd–CNT–rGO nanocomposite. As shown in Figure 3a, Pd NPs are well-dispersed on the surfaces of CNT–rGO nanocomposite (Figure 3a), and the mean particle size is 30 nm from the distribution histogram (Supporting Information Figure S3). It can be observed that the particle size of Pd nanoparticles before hydrothermal reaction (Supporting Information Figure S1b) is much smaller than that of the Pd nanoparticles after the reaction (Figure 3a), and this is because the crystal growth as well as the sintering of Pd nanoparticles will proceed during the hydrothermal reaction. After the hydrothermal treatment, the particle size of Pd nanoparticles increases accordingly. The interplanar spacings for the lattice fringes are 0.225 and 0.196 nm, corresponding to the (111) and (200) lattice planes of face-centered cubic (fcc) Pd structure (Figure 3b). The selected-area electron diffraction (SAED) pattern indicates that the Pd NPs are mainly single-crystalline state (Figure 3c). In addition, the XRD pattern shows the diffraction peaks corresponding to the (002) plane of CNT–

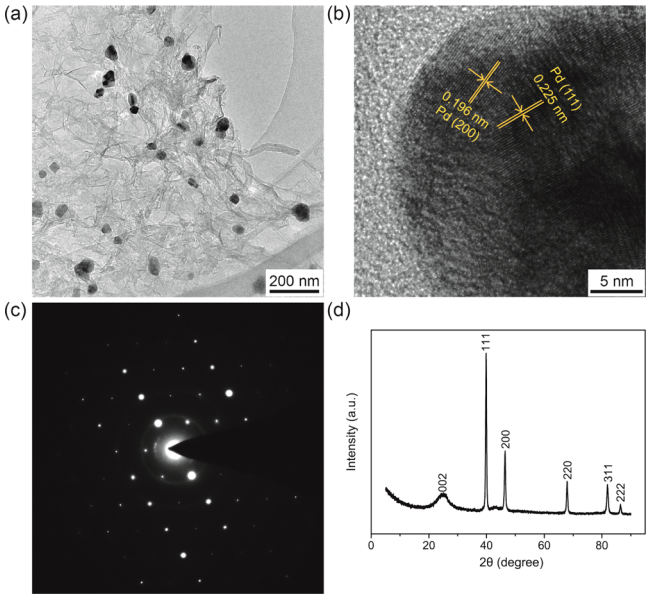

Figure 3. (a,b) TEM images of Pd–CNT–rGO hybrid. (c) SAED pattern and (d) XRD pattern of Pd–CNT–rGO hybrid.

rGO nanocomposite and (111), (200), (220), (311), and (222) planes of Pd NPs (Figure 3d), which also proves that the Pd NPs exhibit a typical fcc pattern of Pd metal.[14]

Figure 4a shows the XPS spectra of Pd–CNT–GO and Pd–CNT–rGO nanohybrid samples. Both exhibit two main peaks centered at about 286 and 532 eV that originated from the graphitic sp^2 carbon atoms and the oxygenate groups, and a weak peak that is assigned to Pd 3d. Typically, the peaks at 284.6, 286.6, and 288.2 eV are attributed to C=C/C–C, C–O, and C=O bonds, respectively.[14] Because of the presence of oxygen-containing functional groups of GO precursor, the peak intensity of the C–O bond in Pd–CNT–GO is as high as 41.91% (Figure 4b). However, in the Pd–CNT–rGO nanohybrid, the peak intensity of the C–O bond tremendously decreases to 22.56%, which demonstrates a high degree of deoxygenation and successful reduction from Pd–CNT–GO to Pd–CNT–rGO during the self-assembly by hydrothermal process (Figure 4c). Furthermore, the core-level XPS signals of Pd 3d in Pd–rGO–CNT samples reveal the Pd $3d_{5/2}$ and $3d_{3/2}$ centered at 335.1 and 340.4 eV, respectively (Figure 4d), which are in good agreement with the reported XPS data of Pd $3d_{5/2}$ and Pd $3d_{3/2}$ in metallic Pd.[28] The Pd content in the catalyst has further been determined using a microwave plasma-atom emission spectrometer, and the result shows that the content of Pd in Pd–CNT–rGO nanocomposite is about 2.98 wt %.

To evaluate the catalytic ability of the synthesized Pd–CNT–rGO nanocatalysts, we have selected the reduction of *p*-nitrophenol to *p*-aminophenol by $NaBH_4$ as a model reaction.[29] The addition of Pd–CNT–rGO nanocatalysts in *p*-nitrophenol aqueous solution causes the fading and ultimate bleaching of the yellow color of the solution. From the UV–vis spectra, it can be observed that the absorption of *p*-nitrophenol at 400 nm decreases quickly, with a concomitant increase of a new peak at 295 nm that is assigned to *p*-aminophenol (Figure 5a). In the presence of Pd–CNT–rGO nanocatalyst, the reduction of *p*-nitrophenol to *p*-aminophenol can be finished in only 30 s, even when the content of Pd in it is as low as 2.98 wt %. The reactions in the presence of $Au@SiO_2$ microsphere,[4] Au@C yolk–shel,l[13] and Au/graphene hydrogel[30] catalysts are finished

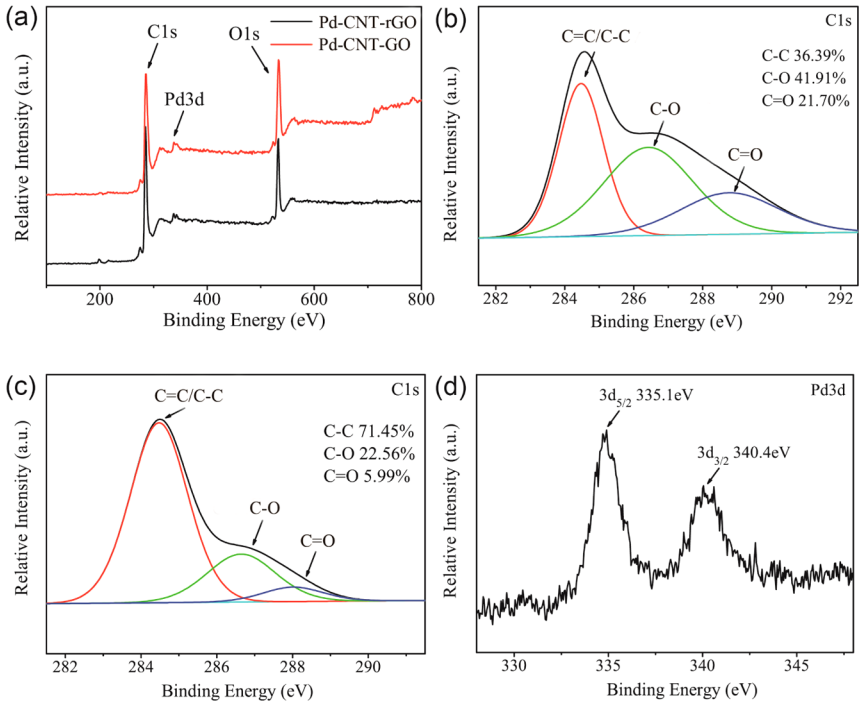

Figure 4. (a) XPS profiles of Pd−CNT−rGO hybrid samples before and after the hydrothermal treatment. (b) Curve fit of the C 1s peak of Pd−CNT−GO precursor and (c) Pd−CNT−rGO hybrid. (d) Curve fit of Pd 3d peak of Pd−CNT−rGO hybrid.

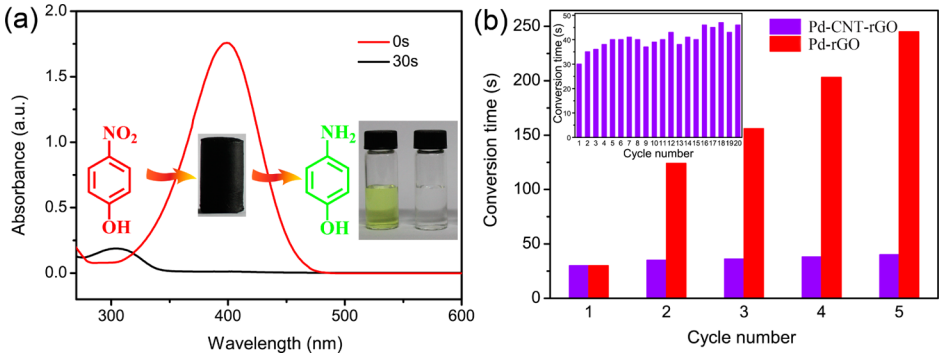

Figure 5. (a) UV/vis spectra of *p*-nitrophenol reduction reaction in the absence and presence of Pd−CNT−rGO catalyst. (b) The stability of Pd−CNT−rGO and Pd−rGO catalysts during five cycles of the same reduction reaction. Inset is the stability of Pd−CNT−rGO nanocatalyst during 20 cycles of the same reduction reaction.

in more than 5 min (Table 1). Furthermore, the turnover frequency (TOF), defined as moles of the reactant (*p*-nitrophenol) converted by per mole of active metal in catalyst per minute, also shows a much higher value for Pd−CNT−rGO hydrogel than that of Au/graphene hydrogel catalyst. Such excellent catalytic activity originated from the introduction of CNTs and the formation of a unique 3D porous structured Pd−CNT−rGO hydrogel. The insertion of hierarchical tortuous CNTs in CNT−rGO nanocomposite can bridge the adjacent graphene nanosheets, which prevent graphene nanosheets from restacking and increase the basal spacing. Thus, the resultant 3D Pd−CNT−rGO hydrogel, which possesses a large surface area and ample volume with hierarchically porous structure, can effectively absorb *p*-nitrophenol via $\pi-\pi$ stacking interactions, and therefore greatly improves the mass-transfer rate and dramatically enhances the catalytic performance of the catalyst. In addition, the introduction of CNTs on the surface of rGO also improves the electron-transfer rate[31] from CNT−rGO scaffold to Pd NPs and provides an electronic active system for the redox reaction of *p*-nitrophenol to *p*-aminophenol by $NaBH_4$, as well as accelerates the reduction rate.

Table 1. Comparison for the Reduction of 4-NP with Different Catalysts

catalyst	metal content (wt %)	conversion time	TOF (min^{-1})	ref
Pd−CNT−rGO	2.98	30 s	0.43	our work
$Au@SiO_2$	NA	60 min	NA	4
Au@C	NA	5 min	NA	13
Au/graphene	24	12 min	0.19	30

The stability of Pd−CNT−rGO nanocatalysts has been investigated by repeated measurements in *p*-nitrophenol under the same condition. After each measurement, the catalyst was recycled by simple filtration and centrifugation, followed by washing with distilled water for the next cycle of catalysis. The Pd−CNT−rGO nanocatalysts exhibit good stability after five

cycles of reactions, with 100% conversion within 40 s reaction periods. Moreover, after 20 successive cycles of reactions, the reaction time can still keep within 46 s (Figure 5b, inset). In comparison, the reduction time with Pd−rGO nanocatalysts increases from 30 to 210 s after five successive cycles of reactions (Figure 5b), giving the Pd−CNT−rGO nanomaterials presented herein great potential as highly effective and stable nanocatalysts.

4. CONCLUSION

3D macroscopic Pd−CNT−rGO hydrogel has been fabricated by a facile one-pot self-assembled approach through the hydrothermal treatment of a mixed aqueous precursor solution of $PdCl_4^{2-}$, CNT, and GO and simultaneously spontaneous redox reaction between $PdCl_4^{2-}$ and CNT−GO hybrid. The resultant Pd−CNT−rGO bifunctional nanocatalyst possesses large surface area and excellent durability, and therefore exhibits remarkably high and stable catalytic activity toward the reduction of *p*-nitrophenol, with 100% conversion within only 30 s. It is anticipated that the optimization of bifunctional components and structural design will significantly further enhance the catalytic properties. Studies of similar bifunctional catalysts syntheses with other catalytically active metals such as Au, Ag, Pt on proper supporting materials, as well as their applications for various chemical reactions, are in progress. Therefore, the proposed facile synthesis route and designed bifunctional catalysts will be a universal platform to fabricate nanocatalysts that can be used in a broad range of catalysis, environmental protection, energy storage, drug delivery, chemical and biological sensing, and so forth.

■ ASSOCIATED CONTENT

Ⓢ Supporting Information

TEM images, nitrogen adsorption/desorption curves, pore size distribution curves, and particle size distribution histogram. This material is available free of charge via the Internet at http://pubs.acs.org.

■ AUTHOR INFORMATION

Corresponding Authors

*E-mail: xiaofei@hust.edu.cn.
*E-mail: zheng.gong@wdc.com.
*E-mail: chmsamuel@mail.hust.edu.cn.

Author Contributions

‖These authors contributed equally.

Notes

The authors declare no competing financial interest.

■ ACKNOWLEDGMENTS

This research was financially supported by the National Natural Science Foundation of China (Project nos. 51173055 and 21305048), and the National Program on Key Basic Research Project (973 Program, Grant no. 2013CBA01600).

■ REFERENCES

(1) Nishihata, Y.; Mizuki, J.; Akao, T.; Tanaka, H.; Uenishi, M.; Kimura, M.; Okamoto, T.; Hamada, N. Self-Regeneration of a Pd-Perovskite Catalyst for Automotive Emissions Control. *Nature* **2002**, *418*, 164−167.

(2) Bianchini, C.; Shen, P. K. Palladium-Based Electrocatalysts for Alcohol Oxidation in Half Cells and in Direct Alcohol Fuel Cells. *Chem. Rev.* **2009**, *109*, 4183−4206.

(3) Balanta, A.; Godard, C.; Claver, C. Pd Nanoparticles for C−C Coupling Reactions. *Chem. Soc. Rev.* **2011**, *40*, 4973−4985.

(4) Lee, J.; Park, J. C.; Song, H. A Nanoreactor Framework of a Au@SiO_2 Yolk/Shell Structure for Catalytic Reduction of p-Nitrophenol. *Adv. Mater.* **2008**, *20*, 1523−1528.

(5) Pileni, M. P. The Role of Soft Colloidal Templates in Controlling the Size and Shape of Inorganic Nanocrystals. *Nat. Mater.* **2003**, *2*, 145−150.

(6) Wilson, O. M.; Scott, R. W. J.; Garcia-Martines, J. C.; Crooks, R. M. Synthesis, Characterization, and Structure-Selective Extraction of 1−3 nm Diameter AuAg Dendrimer-Encapsulated Bimetallic Nanoparticles. *J. Am. Chem. Soc.* **2005**, *127*, 1015−1024.

(7) Lee, Y.; Garcia, M. A.; Frey Huls, N. A.; Sun, S. H. Synthetic Tuning of the Catalytic Properties of Au-Fe_3O_4 Nanoparticles. *Angew. Chem., Int. Ed.* **2010**, *49*, 1293−1296.

(8) Son, S. U.; Jang, Y.; Yoon, K. Y.; Kang, E.; Hyeon, T. Facile Synthesis of Various Phosphine-Stabilized Monodisperse Palladium Nanoparticles Through the Understanding of Coordination Chemistry of the Nanoparticles. *Nano Lett.* **2004**, *4*, 1147−1151.

(9) Choi, H. C.; Shim, M.; Bangsaruntip, S.; Dai, H. J. Spontaneous Reduction of Metal Ions on the Sidewalls of Carbon Nanotubes. *J. Am. Chem. Soc.* **2002**, *124*, 9058−9059.

(10) Qu, L. T.; Dai, L. M. Substrate-Enhanced Electroless Deposition of Metal Nanoparticles on Carbon Nanotubes. *J. Am. Chem. Soc.* **2005**, *127*, 10806−10807.

(11) Arnal, P. M.; Comotti, M.; Schiith, F. High-Temperature-Stable Catalysts by Hollow Sphere Encapsulation. *Angew. Chem., Int. Ed.* **2006**, *45*, 8404−8407.

(12) Ikeda, S.; Ishino, S.; Harada, T.; Okamoto, N.; Sakata, T.; Mori, H.; Kuwabata, S.; Torimoto, T.; Matsumura, M. Ligand-Free Platinum Nanoparticles Encapsulated in a Hollow Porous Carbon Shell as a Highly Active Heterogeneous Hydrogenation Catalyst. *Angew. Chem., Int. Ed.* **2006**, *45*, 7221−7224.

(13) Liu, R.; Mahurin, S. M.; Li, C.; Unocic, R. R.; Idrobo, J. C.; Gao, H. J.; Pennycook, S. J.; Dai, S. Dopamine as a Carbon Source: The Controlled Synthesis of Hollow Carbon Spheres and Yolk Structured Carbon Nanocomposites. *Angew. Chem., Int. Ed.* **2011**, *50*, 6799−6802.

(14) Sun, T.; Zhang, Z. Y.; Xiao, J. W.; Chen, C.; Xiao, F.; Wang, S.; Liu, Y. Q. Facile and Green Synthesis of Palladium Nanoparticles-Graphene-Carbon Nanotube Material with High Catalytic Activity. *Sci. Rep.* **2013**, *3*, 2527.

(15) Ramanathan, T.; Abdala, A. A.; Stankovich, S.; Dikin, D. A.; Herrera-Alonso, M.; Piner, R. D.; Adamson, D. H.; Schniepp, H. C.; Chen, X.; Ruoff, R. S.; Nguyen, S. T.; Aksay, I. A.; Prud'Homme, R. K.; Brinson, L. C. Functionalized Graphene Sheets for Polymer Nanocomposites. *Nat. Nanotechnol.* **2008**, *3*, 327−331.

(16) Shang, L.; Bian, T.; Zhang, B. H.; Zhang, D. H.; Wu, L. Z.; Tung, C. H.; Yin, Y. D.; Zhang, T. R. Graphene-Supported Ultrafine Metal Nanoparticles Encapsulated by Mesoporous Silica: Robust Catalysts for Oxidation and Reduction Reactions. *Angew. Chem., Int. Ed.* **2014**, *126*, 254−258.

(17) Qu, K. G.; Wu, L.; Ren, J. S.; Qu, X. G. Natural DNA-Modified Graphene/Pd Nanoparticles as Highly Active Catalyst for Formic Acid Electro-Oxidation and for the Suzuki Reaction. *ACS Appl. Mater. Interfaces* **2012**, *4*, 5001−5009.

(18) Zhang, Z. Y.; Xiao, F.; Xi, J. B.; Sun, T.; Xiao, S.; Wang, H. R.; Wang, S.; Liu, Y. Q. Encapsulating Pd Nanoparticles in Double Shelled Graphene@Carbon Hollow Spheres for Excellent Chemical Catalytic Property. *Sci. Rep.* **2014**, *4*, 4053.

(19) Kamat, P. V. Graphene-Based Nanoarchitectures. Anchoring Semiconductor and Metal Nanoparticles on a Two-Dimensional Carbon Support. *J. Phys. Chem. Lett.* **2009**, *1*, 520−527.

(20) Hummers, W. S.; Offeman, R. E. Preparation of Graphitic Oxide. *J. Am. Chem. Soc.* **1958**, *80*, 1339.

(21) Zhang, Z. Y.; Xiao, F.; Qian, L. H.; Xiao, J. W.; Wang, S.; Liu, Y. Q. Facile Synthesis of 3D MnO_2-Graphene and Carbon Nanotube-Graphene Composite Networks for High Performance, Flexible, All-Solid-State Asymmetric Supercapacitors. *Adv. Energy Mater.* **2014**, DOI: 10.1002/aenm.201400064.

(22) Kim, J.; Cote, L. J.; Kim, F.; Yuan, W.; Shull, K. R.; Huang, J. X. Graphene Oxide Sheets at Interfaces. *J. Am. Chem. Soc.* **2010**, *132*, 8180−8186.
(23) Chen, X. M.; Wu, G. H.; Chen, J. M.; Chen, X.; Xie, Z. X.; Wang, X. R. Synthesis of "Clean" and Well-Dispersive Pd Nanoparticles with Excellent Electrocatalytic Property on Graphene Oxide. *J. Am. Chem. Soc.* **2011**, *133*, 3693−3695.
(24) Zhou, Y.; Bao, Q. L.; Tang, L. A.; Zhong, Y. L.; Loh, K. P. Hydrothermal Dehydration for the "Green" Reduction of Exfoliated Graphene Oxide to Graphene and Demonstration of Tunable Optical Limiting Properties. *Chem. Mater.* **2009**, *21*, 2950−2956.
(25) Memmingm, R. Photoinduced Charge Transfer Processes at Semiconductor Electrodes and Particles. *Top. Curr. Chem.* **1994**, *169*, 105−107.
(26) Suzuki, S.; Bower, C.; Watanabe, Y.; Zhou, O. Work Functions and Valence Band States of Pristine and Cs-Intercalated Single-Walled Carbon Nanotube Bundles. *Appl. Phys. Lett.* **2000**, *76*, 4007−4009.
(27) Kazaoui, S.; Minami, N.; Matsuda, N. H. H. K.; Achiba, Y. Electrochemical Tuning of Electronic States in Single-Wall Carbon Nanotubes Studied by In Situ Absorption Spectroscopy and Resistance. *Appl. Phys. Lett.* **2001**, *78*, 3433−3435.
(28) Jin, Z.; Nackashi, D.; Lu, W.; Kittrell, C.; Tour, J. M. Decoration, Migration, and Aggregation of Palladium Nanoparticles on Graphene Sheets. *Chem. Mater.* **2010**, *22*, 5695−5699.
(29) Panigrahi, S. B. S.; Praharaj, S.; Pande, S.; Jana, S.; Pal, A.; Ghosh, S. K.; Pal, T. Synthesis and Size-Selective Catalysis by Supported Gold Nanoparticles: Study on Heterogeneous and Homogeneous Catalytic Process. *J. Phys. Chem. C* **2007**, *111*, 4596−4605.
(30) Li, J.; Liu, C. Y.; Liu, Y. Au/Graphene Hydrogel: Synthesis, Characterization and Its Use for Catalytic Reduction of 4-Nitrophenol. *J. Mater. Chem.* **2012**, *22*, 8426−8430.
(31) Tung, V. C.; Huang, J. H.; Tevis, I.; Kim, F.; Kim, J.; Chu, C. W.; Stupp, S. I.; Huang, J. X. Surfactant-Free Water Processable Photoconductive All-Carbon Composite. *J. Am. Chem. Soc.* **2011**, *133*, 4940−4947.